


Alternative derivation of Mie theory with electromagnetic potentials for diffuse particlesM. Houtput,¹ N. Van den Broeck,¹ F. Brosens,¹ M. Morshed Behbahani,² and J. Tempere¹¹*Theory of Quantum Systems and Complex Systems, Universiteit Antwerpen, B-2000 Antwerpen, Belgium*²*Fundamental Interactions and Symmetries, Rijksuniversiteit Groningen, 9747 AA Groningen, The Netherlands* (Received 10 May 2019; revised manuscript received 19 November 2019; published 5 December 2019)

Mie's theory of light scattering on spherical particles is being increasingly used in nanophotonics, and these demanding applications have laid bare some shortcomings of Mie theory in its standard formulation. One problem that deserves special attention is the electron spill-out in small metallic nanoparticles, which invalidates the assumption of an abrupt interface. Here we present an alternative derivation of Mie theory without this assumption. To avoid the usual electromagnetic boundary conditions suitable for a hard-wall interface, we set up equations for the electromagnetic potentials instead of the electric and magnetic field. We show that in the limit of a hard-wall interface, the results of the standard Mie theory are recovered. Additionally, a numerical solution scheme is proposed for the equations for the vector potential and the scalar potential. Analysis of the optical cross sections of soft-interface nanospheres shows that the absorption increases and occurs at lower frequencies as compared to hard-walled nanospheres. This effect is rather dramatic in large spheres with large spill-out, due to the disappearance of high-frequency resonance peaks.

DOI: [10.1103/PhysRevB.100.235409](https://doi.org/10.1103/PhysRevB.100.235409)**I. INTRODUCTION**

In this paper we rederive Mie theory [1] for the scattering of light by a spherical particle in an alternative way. The reader may very well wonder what the use is of yet another derivation of Mie theory, given that there are already very good and thorough presentations in standard textbooks such as that of Stratton [2], Kerker [3], or more recently Kreibig and Vollmer [4], and Bohren and Huffman [5]. The answer to that question is that we provide a derivation based on the scalar potential ϕ and the vector potential \mathbf{A} , rather than the electric and magnetic fields \mathbf{E} and \mathbf{B} , or other potentials such as the Hertz-Debye potentials [3]. This approach allows for a straightforward extension to smeared out interfaces between materials, allowing us to reproduce the results from Wyatt's extension for inhomogeneous nanospheres [6,7]. The derivation directly considers the electronic response to an external electric field rather than assuming a dielectric response function for the medium, which is in line with other treatments of the problem that use a nonlocal response [8–11]. Additionally, since we can associate the scalar potential with the longitudinal fields and the vector potential with the transversal fields, this rederivation can provide an insight into Ruppin's extension for plasma spheres [12–14]. Finally, a numerical solution of the equations that follow from our derivation allows for an efficient calculation of the optical cross sections taking spill-out into account.

In standard Mie theory, only transverse electromagnetic waves with a divergence-free electric field are considered. However, in a metal the (longitudinal) plasma oscillations couple to the radiation field, and the longitudinal modes of the field need to be taken into account. For bulk metal, the plasma frequency is much higher than the optical frequencies and a description based only on transverse fields is adequate. However, for small particles, the surface plasma modes

become important and affect the optical properties. This was first shown by Melnyk and Harrison [15], and Mie theory was subsequently extended to include longitudinal fields by Ruppin [12–14].

Additionally, Mie assumed the boundary between the inside of the spherical particle and the outside to be infinitely sharp, in order to implement the usual electromagnetic boundary conditions that link regions with different uniform bulk dielectric response. However, there are plenty of cases where this assumption is inapplicable [16]. A first example appears when light-absorbing nanoparticles are used as heaters [17]: due to the gradient in temperature, the surrounding material will be characterized by a smoothly varying, nonuniform dielectric response. When the variation of the dielectric function occurs on a length scale comparable to the wavelength, it is no longer possible to treat this system as an “onion” of successive shells with constant permittivity in each shell [18], and standard (multilayer) Mie theory breaks down [19]. Additionally, in these applications it is often important to maximize the absorption of the nanoparticles, which is done by adjusting parameters such as size and shape. The “smoothness” of the nanoparticle also influences absorption, and could possibly be adjusted to increase absorption as well. A second example where standard Mie theory fails can be found in nanoplasmonics: for very small metallic spheres the electron spill-out effect causes the charge density to vary gradually through the interface, and this leads to a shift in the plasma resonance frequencies [8]. This effect has been captured thus far only with a hydrodynamic theory for the electron fluid, which gives the locations of the resonances but not their width. Up until now, the variation in the dielectric function has only been investigated for length scales comparable to the electron spill-out length, an unnecessary restriction that needs to be lifted when looking at applications where the smoothness can be arbitrarily adjusted. It is noteworthy that scattering of

microwave radiation off of a metamaterial [20–22] provides an interesting platform for this artificial spill-out. Since the properties of a metamaterial can be chosen locally [23], one could make a spherical particle that has a radially varying dielectric function and relative permeability, essentially mimicking the effect of a smooth electron density that can be arbitrarily chosen. The feasibility of such an experiment is demonstrated by [24], where the microwave scattering from a hard-walled metamaterial sphere is experimentally measured.

The focus of this paper lies on the extension of Mie theory to smooth interfaces. The paper is structured as follows. In Sec. II we derive our theory for light scattering of spherically symmetric systems that allows us to take into account any local linear dielectric response that varies smoothly in the radial direction. In the limit of abrupt interfaces, this theory recovers the standard Mie theory, as shown in Sec. III. A numerical scheme to find the scalar and vector potentials of a soft-walled nanosphere is introduced in Sec. IV. This scheme is used to investigate the influence of boundary softening on the optical cross sections in Sec. V. Finally, we discuss and summarize the results in Sec. VI.

II. SCATTERING OF LIGHT ON “SOFT” SPHERICAL INTERFACES

A. Overview of the calculational scheme

In the presence of a material, the scalar and vector potentials are split into induced and external fields, $\phi = \phi^{\text{ind}} + \phi^{\text{ext}}$, and $\mathbf{A} = \mathbf{A}^{\text{ind}} + \mathbf{A}^{\text{ext}}$. The external field will represent the incoming light that scatters on the spherical particle. The scheme of the calculation is as follows: the total fields ϕ , \mathbf{A} will induce charges ρ^{ind} and currents \mathbf{J}^{ind} in the material, as dictated by the response theory for the material. These in turn give rise to the induced fields ϕ^{ind} , \mathbf{A}^{ind} as dictated by the Maxwell equations, and these induced fields are fed back into the total fields ϕ , \mathbf{A} . This calculation scheme leads to self-consistent equations for the induced fields, and solving these equations solves the scattering problem.

In this scheme we take into account a smoothly varying density of charge carriers through a “local approximation.” Given the response of a uniform system of (free or bound) charge carriers at a bulk density n_0 , we find the response of a system with smoothly varying density profile $n(\mathbf{r}) = n_0 f(\mathbf{r})$ by scaling the bulk response with $f(\mathbf{r})$, the ratio of local density to bulk density of charge carriers. This local approximation for the charge carriers is valid as long as the density variations of the charge carriers occur on a length scale δ much larger than the inverse Fermi wave number $k_F \delta \gg 1$. For metallic particles, k_F is of the order of inverse angstrom, so that density variations on the length scale of optical or even UV wavelengths easily satisfy the requirement for the local approximation.

B. Self-consistent equation for the induced fields

We describe the charge carriers in the metal by a continuum model, and indicate the displacement of the charge carriers at position \mathbf{r} and time t by a “strain” field $\mathbf{u}(\mathbf{r}, t)$. The total charge displacement at \mathbf{r} is then $n(\mathbf{r})\mathbf{u}(\mathbf{r}, t)$. The induced

charge density and charge current density are described by the following equations:

$$\rho^{\text{ind}}(\mathbf{r}, t) = -\nabla \cdot [n(\mathbf{r})\mathbf{u}(\mathbf{r}, t)], \quad (1)$$

$$\mathbf{J}^{\text{ind}}(\mathbf{r}, t) = n(\mathbf{r})\dot{\mathbf{u}}(\mathbf{r}, t). \quad (2)$$

Moreover, we restrict our discussion to (1) *monochromatic* light (of a given frequency ω) and (2) *local linear* response theories. The former assumption provides the various fields with a time dependence proportional to $e^{-i\omega t}$. The latter assumption allows us to link the charge displacement to the total electric field through

$$n_0\mathbf{u}(\mathbf{r}, \omega) = \varepsilon_0\chi(\omega)\mathbf{E}(\mathbf{r}, \omega), \quad (3)$$

with ε_0 the vacuum permittivity (we work in SI units). The prefactor n_0 ensures that χ can be interpreted as the *bulk susceptibility* corresponding to the chosen response theory. More general nonlocal response theories are possible [9,11,25] if we relax the local approximation described earlier; however, here we consider local response for simplicity.

The commonly used Drude model for the susceptibility fits in the above response formula (3). Indeed, it can be derived from the equation of motion for the charge carriers:

$$m\frac{\partial^2\mathbf{u}(\mathbf{r}, t)}{\partial t^2} + \frac{m}{\tau}\frac{\partial\mathbf{u}(\mathbf{r}, t)}{\partial t} = -e\mathbf{E}(\mathbf{r}, t), \quad (4)$$

where the second term is the phenomenological friction term, which defines the Drude relaxation time τ . Here we neglected the magnetic contribution to the Lorentz force, which is a second order term. Using the time dependence $e^{-i\omega t}$, we get $\mathbf{u}(\mathbf{r}, \omega) \sim \mathbf{E}(\mathbf{r}, \omega)$, which is in the form of (3). The susceptibility can be readily extracted:

$$\chi(\omega) = -\frac{\frac{n_0 e^2}{m\varepsilon_0}}{\omega^2 + i\frac{\omega}{\tau}} := -\frac{\omega_{\text{pl}}^2}{\omega^2 + i\frac{\omega}{\tau}}, \quad (5)$$

where ω_{pl} is the plasma frequency. For the remainder of this section, we will use a general response function $\chi(\omega)$, but for all results the Drude model will be used.

Combining formulas (2) and (3), we obtain the local induced current $\mathbf{J}^{\text{ind}}(\mathbf{r}, \omega)$, which is equal to the induced current for the bulk rescaled by the factor $f(\mathbf{r}) = n(\mathbf{r})/n_0$:

$$\mathbf{J}^{\text{ind}}(\mathbf{r}, \omega) = -i\omega\varepsilon_0 f(\mathbf{r})\chi(\omega)\mathbf{E}(\mathbf{r}, \omega). \quad (6)$$

The above equation describes the current induced by the displacement of charges, so that this description does not include mechanisms for transverse response. Indeed, the transverse or divergence-free component of the current is not linked to charge motion, as is clear from the continuity equation.

The electromagnetic potentials are introduced with the following definition:

$$\mathbf{E}(\mathbf{r}, \omega) = -\nabla\phi(\mathbf{r}, \omega) + i\omega\mathbf{A}(\mathbf{r}, \omega). \quad (7)$$

Here we will use the Coulomb (or “transverse”) gauge

$$\nabla \cdot \mathbf{A}(\mathbf{r}, \omega) = 0. \quad (8)$$

From here on, we will stop writing the ω dependence of all functions explicitly.

Substituting (7) into (6), and using the continuity equation

$$i\omega\rho^{\text{ind}}(\mathbf{r}) = \nabla \cdot \mathbf{J}^{\text{ind}}(\mathbf{r}), \quad (9)$$

the following expressions for the induced charge density and charge current density are obtained:

$$\rho^{\text{ind}}(\mathbf{r}) = \varepsilon_0 \nabla \cdot \{\chi f(\mathbf{r})[\nabla\phi(\mathbf{r}) - i\omega\mathbf{A}(\mathbf{r})]\}, \quad (10)$$

$$\mathbf{J}^{\text{ind}}(\mathbf{r}) = i\omega\varepsilon_0\chi f(\mathbf{r})[\nabla\phi(\mathbf{r}) - i\omega\mathbf{A}(\mathbf{r})]. \quad (11)$$

The induced charges and currents give rise to the induced scalar and vector potential according to the Maxwell equations (in SI units):

$$\Delta\phi^{\text{ind}}(\mathbf{r}) = -\frac{\rho^{\text{ind}}(\mathbf{r})}{\varepsilon_0}, \quad (12)$$

$$\left(\Delta + \frac{\omega^2}{c^2}\right)\mathbf{A}^{\text{ind}}(\mathbf{r}) = -\mu_0\mathbf{J}^{\text{ind}}(\mathbf{r}) - i\frac{\omega}{c^2}\nabla\phi^{\text{ind}}(\mathbf{r}). \quad (13)$$

Here c is the speed of light in vacuum and μ_0 is the vacuum permeability. Substituting (10) and (11) into these equations, we get

$$\Delta\phi^{\text{ind}}(\mathbf{r}) = -\nabla \cdot \{\chi f(\mathbf{r})[\nabla\phi(\mathbf{r}) - i\omega\mathbf{A}(\mathbf{r})]\}, \quad (14)$$

$$\begin{aligned} \left(\Delta + \frac{\omega^2}{c^2}\right)\mathbf{A}^{\text{ind}}(\mathbf{r}) = & -i\frac{\omega}{c^2}\chi f(\mathbf{r})[\nabla\phi(\mathbf{r}) - i\omega\mathbf{A}(\mathbf{r})] \\ & - i\frac{\omega}{c^2}\nabla\phi^{\text{ind}}(\mathbf{r}). \end{aligned} \quad (15)$$

In these equations the total scalar and vector potentials contain the induced potentials via $\phi = \phi^{\text{ind}} + \phi^{\text{ext}}$ and $\mathbf{A} = \mathbf{A}^{\text{ind}} + \mathbf{A}^{\text{ext}}$. Note that whenever boundaries or inhomogeneities are present, $\nabla f(\mathbf{r}) \neq 0$ and the right-hand side of Eq. (14) is nonzero. In this case the equations are coupled. This ensures that even for a purely transverse external perturbation ($\phi^{\text{ext}} = 0$), the system can respond with both longitudinal and transverse induced fields. Hence, only in the case of a uniform, infinite system [i.e., $\nabla f(\mathbf{r}) = 0$ everywhere] will a transverse perturbation lead to a purely transverse response. For a hard-walled nanosphere [i.e., $f(\mathbf{r}) = \Theta(R - |\mathbf{r}|)$ with Θ the Heaviside function] the coupling occurs through the values at the interface $|\mathbf{r}| = R$, as discussed in Sec. III.

C. Equations for the spherical vector harmonic components

For the remainder of the article we will turn our attention to spherically symmetric scatterers, such as nanospheres. This means the density profile varies only in the radial direction, so we write $f(r)$ from now on. Exploiting the spherical symmetry of the scatterer allows us to simplify Eqs. (14) and (15), using an expansion in spherical harmonics. Rather than using the $\mathbf{L}, \mathbf{M}, \mathbf{N}$ vector spherical harmonics defined in Stratton [2], we use the $\mathbf{Y}, \mathbf{\Psi}, \mathbf{\Phi}$ vector spherical harmonics introduced by Barrera *et al.* [26]:

$$\mathbf{Y}_{\ell,m}(\theta, \varphi) = Y_{\ell,m}(\theta, \varphi)\mathbf{e}_r, \quad (16)$$

$$\mathbf{\Psi}_{\ell,m}(\theta, \varphi) = r\nabla Y_{\ell,m}(\theta, \varphi), \quad (17)$$

$$\mathbf{\Phi}_{\ell,m}(\theta, \varphi) = \mathbf{r} \times \nabla Y_{\ell,m}(\theta, \varphi), \quad (18)$$

where \mathbf{r} is the position vector, and $Y_{\ell,m}(\theta, \varphi)$ is the spherical harmonic function. Some properties of this basis are listed in Table I. In this work we choose the convention

$$Y_{\ell,-m}(\theta, \varphi) = (-1)^m Y_{\ell,m}^*(\theta, \varphi) \quad (19)$$

to define negative m spherical harmonics. This means the Condon-Schortley phase factor appears in the modified Legendre polynomials,

$$P_\ell^m(x) = (-1)^m (1-x^2)^{m/2} \frac{d^m P_\ell(x)}{dx^m}, \quad \text{where } m \geq 0. \quad (20)$$

The triplet of vectors $\mathbf{Y}, \mathbf{\Psi}, \mathbf{\Phi}$ forms an orthogonal basis at any position \mathbf{r} , such that $\mathbf{Y}_{\ell,m}$ is directed along the radial direction. Any vector field can be decomposed in this basis, and we can write the potentials as

$$\begin{aligned} \mathbf{A}(\mathbf{r}) = & \sum_{\ell=0}^{\infty} \sum_{m=-\ell}^{\ell} [A_{\ell,m}^Y(r)\mathbf{Y}_{\ell,m}(\theta, \varphi) + A_{\ell,m}^\Psi(r)\mathbf{\Psi}_{\ell,m}(\theta, \varphi) \\ & + A_{\ell,m}^\Phi(r)\mathbf{\Phi}_{\ell,m}(\theta, \varphi)], \end{aligned} \quad (21)$$

$$\phi(\mathbf{r}) = \sum_{\ell=0}^{\infty} \sum_{m=-\ell}^{\ell} \phi_{\ell,m}(r)Y_{\ell,m}(\theta, \varphi). \quad (22)$$

If we define the two following differential operators:

$$\hat{L}_l^\Phi[f(r)] = \frac{\partial^2 f}{\partial r^2} + \frac{2}{r} \frac{\partial f}{\partial r} - \frac{\ell(\ell+1)}{r^2} f(r), \quad (23)$$

$$\hat{L}_l^Y[f(r)] = \frac{\partial^2 f}{\partial r^2} + \frac{4}{r} \frac{\partial f}{\partial r} - \frac{(\ell-1)(\ell+2)}{r^2} f(r), \quad (24)$$

then using the properties of Table I, Eqs. (14) and (15) result in the following equations for the components of the scalar potential:

$$\begin{aligned} [1 + \chi f(r)]\hat{L}_l^\Phi[\phi_{\ell,m}^{\text{ind}}(r)] + \chi \frac{\partial f}{\partial r} \frac{\partial \phi_{\ell,m}^{\text{ind}}}{\partial r} \\ = i\omega\chi \frac{\partial f}{\partial r} [A_{\ell,m}^{\text{ind},Y}(r) + A_{\ell,m}^{\text{ext},Y}(r)], \end{aligned} \quad (25)$$

for the Y components of the vector potential:

$$\begin{aligned} \hat{L}_l^Y[A_{\ell,m}^{\text{ind},Y}(r)] + \frac{\omega^2}{c^2} [1 + \chi f(r)]A_{\ell,m}^{\text{ind},Y}(r) \\ = -\frac{\omega^2}{c^2} \chi f(r)A_{\ell,m}^{\text{ext},Y}(r) - i\frac{\omega}{c^2} [1 + \chi f(r)] \frac{\partial \phi_{\ell,m}^{\text{ind}}}{\partial r}, \end{aligned} \quad (26)$$

and for the Φ components of the vector potential:

$$\begin{aligned} \hat{L}_l^\Phi[A_{\ell,m}^{\text{ind},\Phi}(r)] + \frac{\omega^2}{c^2} [1 + \chi f(r)]A_{\ell,m}^{\text{ind},\Phi}(r) \\ = -\frac{\omega^2}{c^2} \chi f(r)A_{\ell,m}^{\text{ext},\Phi}(r). \end{aligned} \quad (27)$$

The Ψ component is directly linked to the Y component through

$$A_{\ell,m}^\Psi(r) = \frac{1}{r\ell(\ell+1)} \frac{\partial}{\partial r} [r^2 A_{\ell,m}^Y(r)], \quad (28)$$

as to satisfy the Coulomb gauge (8).

Given the external perturbation and a radial density profile function $f(r)$ for the charge carriers (free or bound), the

TABLE I. An overview of the properties of the vector spherical harmonic basis \mathbf{Y} , $\mathbf{\Psi}$, $\mathbf{\Phi}$ used in this work. Here $F = F(r)$ represents a scalar function of the radial distance, and $\int \cdots d\Omega$ represents integration over the angular coordinates, with $d\Omega = \sin\theta d\theta d\varphi$.

Properties of vector spherical harmonics \mathbf{Y} , $\mathbf{\Psi}$, $\mathbf{\Phi}$	
$\mathbf{Y}_{\ell,-m} = (-1)^m \mathbf{Y}_{\ell,m}^*$	$\mathbf{Y}_{\ell,m} \cdot \mathbf{\Psi}_{\ell,m} = 0$
$\mathbf{\Psi}_{\ell,-m} = (-1)^m \mathbf{\Psi}_{\ell,m}^*$	$\mathbf{Y}_{\ell,m} \cdot \mathbf{\Phi}_{\ell,m} = 0$
$\mathbf{\Phi}_{\ell,-m} = (-1)^m \mathbf{\Phi}_{\ell,m}^*$	$\mathbf{\Psi}_{\ell,m} \cdot \mathbf{\Phi}_{\ell,m} = 0$
$\int \mathbf{Y}_{\ell,m} \cdot \mathbf{Y}_{\ell',m'}^* d\Omega = \delta_{\ell,\ell'} \delta_{m,m'}$	$\int \mathbf{Y}_{\ell,m} \cdot \mathbf{\Psi}_{\ell',m'}^* d\Omega = 0$
$\int \mathbf{\Psi}_{\ell,m} \cdot \mathbf{\Psi}_{\ell',m'}^* d\Omega = \ell(\ell+1) \delta_{\ell,\ell'} \delta_{m,m'}$	$\int \mathbf{Y}_{\ell,m} \cdot \mathbf{\Phi}_{\ell',m'}^* d\Omega = 0$
$\int \mathbf{\Phi}_{\ell,m} \cdot \mathbf{\Phi}_{\ell',m'}^* d\Omega = \ell(\ell+1) \delta_{\ell,\ell'} \delta_{m,m'}$	$\int \mathbf{\Psi}_{\ell,m} \cdot \mathbf{\Phi}_{\ell',m'}^* d\Omega = 0$
$\nabla(F\mathbf{Y}_{\ell,m}) = \frac{dF}{dr} \mathbf{Y}_{\ell,m} + \frac{F}{r} \mathbf{\Psi}_{\ell,m}$	$\Delta(F\mathbf{Y}_{\ell,m}) = \left(\frac{1}{r^2} \frac{d}{dr} (r^2 \frac{d}{dr} F) - \frac{\ell(\ell+1)}{r^2} F\right) \mathbf{Y}_{\ell,m}$
$\nabla \cdot (F\mathbf{Y}_{\ell,m}) = \frac{1}{r^2} \frac{d}{dr} (r^2 F) Y_{\ell,m}$	$\nabla \times (F\mathbf{Y}_{\ell,m}) = -\frac{1}{r} F \mathbf{\Phi}_{\ell,m}$
$\nabla \cdot (F\mathbf{\Psi}_{\ell,m}) = -\frac{\ell(\ell+1)}{r} F Y_{\ell,m}$	$\nabla \times (F\mathbf{\Psi}_{\ell,m}) = \frac{1}{r} \frac{d}{dr} (rF) \mathbf{\Phi}_{\ell,m}$
$\nabla \cdot (F\mathbf{\Phi}_{\ell,m}) = 0$	$\nabla \times (F\mathbf{\Phi}_{\ell,m}) = -\frac{\ell(\ell+1)}{r} F \mathbf{Y}_{\ell,m} - \frac{1}{r} \frac{d}{dr} (rF) \mathbf{\Psi}_{\ell,m}$

solution of the set of Eqs. (25)–(28) provides the induced fields \mathbf{A}^{ind} and ϕ^{ind} . Equations (25)–(28) and their numerical implementation, as outlined below, are the key results of the current paper. Since the external perturbation is an electromagnetic wave, $\phi^{\text{ext}} = 0$ and $\phi = \phi^{\text{ind}}$. From here on, we drop the superscript “ind.” For a general density profile $f(r)$, these equations have to be solved numerically. Note that in Eq. (25) for the scalar potential, the vector potential does not drop out when the density gradient is different from zero: a term $(\nabla f) \cdot \mathbf{A}$ remains, in contrast to other treatments of Mie for diffuse surfaces [6,7]. Also when the interface is abrupt, the value of the vector potential at the interface will influence the equation for the scalar potential.

For the external field, we will use a plane wave, coming in from the negative z axis, and polarized such that the electric field lies along the x axis:

$$\mathbf{A}^{\text{ext}} = A_0 e^{ikz} \mathbf{e}_x. \quad (29)$$

When decomposed in vector spherical harmonics [27], the components become

$$A_{\ell,m}^{\text{ext},Y}(r) = \alpha_{\ell,m} \frac{j_\ell(kr)}{kr}, \quad (30)$$

$$A_{\ell,m}^{\text{ext},\Phi}(r) = \beta_{\ell,m} j_\ell(kr), \quad (31)$$

$$A_{\ell,m}^{\text{ext},\Psi}(r) = \frac{\alpha_{\ell,m}}{\ell(\ell+1)} \left[\frac{j_\ell(kr)}{kr} + j'_\ell(kr) \right], \quad (32)$$

where we have defined the following two coefficients:

$$\alpha_{\ell,m} := i^{\ell+1} A_0 (\delta_{m,1} - \delta_{m,-1}) \sqrt{\pi \ell(\ell+1)(2\ell+1)}, \quad (33)$$

$$\beta_{\ell,m} := -i^{\ell+1} A_0 (\delta_{m,1} + \delta_{m,-1}) \sqrt{\pi \frac{2\ell+1}{\ell(\ell+1)}}. \quad (34)$$

In these expressions, $j_\ell(x)$ is the spherical Bessel function of the first kind and of order ℓ , and $j'_\ell(x)$ is its derivative with respect to the argument x . Furthermore, $k = \omega/c$ with c the speed of light in vacuum.

III. MIE THEORY AS THE HARD-WALL LIMIT

A. Solution for the scalar potential

From here on, we focus on a simple Drude-type response, i.e.,

$$\chi(\omega) = -\frac{\omega_{\text{pl}}^2}{\omega(\omega + i/\tau)}. \quad (35)$$

In the limiting case of an abrupt interface at $r = R$, the profile function can be represented by a step function at $r = R$, yielding $f(r) = \Theta(R - r)$. Equation (25) for the scalar potential becomes

$$\begin{aligned} [1 + \Theta(R - r)\chi] \left(\frac{\partial^2}{\partial r^2} + \frac{2}{r} \frac{\partial}{\partial r} - \frac{\ell(\ell+1)}{r^2} \right) \phi_{\ell,m}(r) \\ = \frac{\partial \Theta(R - r)}{\partial r} \left(i\omega \chi A_{\ell,m}^Y(r) - \chi \frac{\partial \phi_{\ell,m}}{\partial r} \right). \end{aligned} \quad (36)$$

This differential equation can be solved with the method of the variation of coefficients, both inside and outside the radius R . The derivative of the step function is then removed by partial integration. The result is

$$\phi_{\ell,m}(r) = \left[\frac{r^\ell}{R^\ell} \Theta(R - r) + \frac{R^{\ell+1}}{r^{\ell+1}} \Theta(r - R) \right] \frac{i\omega \chi R A_{\ell,m}^Y(R)}{2\ell + 1 + \ell \chi}. \quad (37)$$

In our formalism, it is the change in density at the surface that leads to a longitudinal response (a scalar potential) when the system is subjected to a purely transverse perturbation. The induced charge can accumulate on the edge of the nanoparticle, giving rise to a scalar potential. In the result (37), the total vector potential appears, so the result is not complete without a calculation of the induced vector potential from Eq. (26).

B. Solution for the Y component of the vector potential

For both of the vector potential equations, the problem reduces to finding the eigenfunctions of the differential operators \hat{L}_l^Y and \hat{L}_l^Φ , since both inside and outside the sphere $f(r)$ can be considered constant. The eigenfunctions of \hat{L}_l^Y are

cylinder functions divided by their argument, as well as two Euler-type solutions:

$$\hat{L}_\ell^Y \left[\frac{C_\ell(ax)}{ax} \right] = -a^2 \frac{C_\ell(ax)}{ax}, \quad (38)$$

$$\hat{L}_\ell^Y [r^{\ell+1}] = 0, \quad (39)$$

$$\hat{L}_\ell^Y \left[\frac{1}{r^{\ell+2}} \right] = 0, \quad (40)$$

where $C_\ell(x)$ stands for any of the following: the spherical Bessel function $j_\ell(x)$, the spherical Neumann function $y_\ell(x)$, the spherical Hankel functions of the first kind $h_\ell(x)$, and that of the second kind $h_\ell^{(2)}(x)$. These will constitute solutions of the homogeneous equation for $A_{\ell,m}^{\text{ind},Y}(r)$. Inside the sphere, we exclude the divergent part $y_\ell(x)$ and retain $j_\ell(x)$. Outside the sphere, we exclude incoming spherical waves $h_\ell^{(2)}$ outside the sphere, and keep $h_\ell(x)$. The particular solution can be found by noting that the external Y field (30) is an eigenfunction of \hat{L}_ℓ^Y . Using the solution (37) for the scalar potential in Eq. (26), it is straightforward to show that the solutions inside and outside the sphere are given by

$$A_{\ell,m}^{\text{ind},Y}(r < R) = C_{<} \frac{j_\ell(\kappa r)}{\kappa r} - A_{\ell,m}^{\text{ext},Y}(r) + \frac{\ell\chi}{2\ell+1+\ell\chi} A_{\ell,m}^Y(R) \frac{r^{\ell-1}}{R^{\ell-1}}, \quad (41)$$

$$A_{\ell,m}^{\text{ind},Y}(r > R) = C_{>} \frac{h_\ell(\kappa r)}{\kappa r} - \frac{(\ell+1)\chi}{2\ell+1+\ell\chi} A_{\ell,m}^Y(R) \frac{R^{\ell+2}}{r^{\ell+2}}, \quad (42)$$

where we defined $\kappa^2 = k^2(1+\chi)$, and $C_{>}$ and $C_{<}$ are integration constants. These are found by demanding continuity of $A_{\ell,m}^{\text{ind},Y}(r)$ and of its first derivative at the interface $r = R$. Solving the resulting 2×2 system of equations, we find

$$C_{<} = -\alpha_{\ell m} \frac{i\kappa}{k\xi_\ell(\kappa R)\psi'_\ell(\kappa R) - \kappa\psi_\ell(\kappa R)\xi'_\ell(\kappa R)} \quad (43)$$

and

$$C_{>} = -\alpha_{\ell m} \frac{\kappa\psi_\ell(\kappa R)\psi'_\ell(\kappa R) - k\psi_\ell(\kappa R)\psi'_\ell(\kappa R)}{\kappa\psi_\ell(\kappa R)\xi'_\ell(\kappa R) - k\xi_\ell(\kappa R)\psi'_\ell(\kappa R)}, \quad (44)$$

where we expressed the solutions in terms of Ricatti-Bessel functions $\psi_\ell(x) = xj_\ell(x)$ and $\xi_\ell(x) = xh_\ell(x)$. These coefficients are identical to those of Mie theory, confirming the correspondence between our theory and Mie theory.

C. Solution for the Φ component of the vector potential

Finally, we turn to the equation for the Φ component of the vector potential. The operator \hat{L}_ℓ^Φ has the cylinder functions as eigenfunctions:

$$\hat{L}_\ell^\Phi [C_\ell(ax)] = -a^2 C_\ell(ax). \quad (45)$$

Therefore, in a very similar fashion to the Y component, we straightforwardly find the following solutions:

$$A_{\ell,m}^{\text{ind},\Phi}(r < R) = B_{<} j_\ell(\kappa r) - \beta_{\ell m} j_\ell(\kappa r), \quad (46)$$

$$A_{\ell,m}^{\text{ind},\Phi}(r > R) = B_{>} h_\ell(\kappa r), \quad (47)$$

where the integration constants are $B_{<}$ and $B_{>}$. These are found as in the previous case by requiring continuity of $A_{\ell,m}^{\text{ind},\Phi}(r)$ and its first derivative at the boundary $r = R$. We obtain

$$B_{<} = -\beta_{\ell m} \frac{i\kappa}{\kappa\xi_\ell(\kappa R)\psi'_\ell(\kappa R) - \kappa\psi_\ell(\kappa R)\xi'_\ell(\kappa R)} \quad (48)$$

and

$$B_{>} = -\beta_{\ell m} \frac{kj_\ell(\kappa R)j'_\ell(\kappa R) - \kappa j_\ell(\kappa R)j'_\ell(\kappa R)}{kj_\ell(\kappa R)h'_\ell(\kappa R) - \kappa h_\ell(\kappa R)j'_\ell(\kappa R)}. \quad (49)$$

The results (48) and (49) correspond to the results of standard Mie theory for the ‘‘magnetic’’ Φ mode. Finally, it is possible to calculate the optical cross sections using only the coefficients $B_{>}$ and $C_{>}$, using a formula that is identical to the one used in Mie theory.

D. Near-field solution

The resulting electric field given by Eq. (7) close to the metal sphere is shown in Fig. 1. The near field is exactly the same as that obtained from Mie theory. This is a necessary consistency check, since we do not impose the usual electromagnetic boundary conditions. Rather, we use the limit of a continuous profile function $f(r)$. Physically, it is not obvious that these two methods give the same result, especially since the infinitely sharp density variation in the step function violates the local approximation we used to derive our equations. However, it can be proven that the usual electromagnetic boundary conditions follow from Eqs. (7), (14), and (15) in general, assuming the potentials themselves are continuous. This explains the success of both methods.

IV. NUMERICAL SOLUTION OF THE FIELD EQUATIONS

A. Finite difference method

In order to obtain results for a general density profile $f(r)$, Eqs. (25)–(28) have to be solved numerically. This is most easily done by discretization of the equations on an inhomogeneous grid r_j with N grid points. Let $\mathcal{F}(r)$ be any of the functions $\phi_{\ell,m}(r)$, $A_{\ell,m}^{\text{ind},Y}(r)$, $A_{\ell,m}^{\text{ind},\Phi}(r)$, $A_{\ell,m}^{\text{ind},\Psi}(r)$, and call $\mathcal{F}(r_j) := \mathcal{F}_j$, then the derivatives of $\mathcal{F}(r)$ are discretized as follows:

$$\left. \frac{\partial \mathcal{F}}{\partial r} \right|_{r_j} \approx \frac{r_j - r_{j-1}}{r_{j+1} - r_{j-1}} \left(\frac{\mathcal{F}_{j+1} - \mathcal{F}_j}{r_{j+1} - r_j} \right) + \frac{r_{j+1} - r_j}{r_{j+1} - r_{j-1}} \left(\frac{\mathcal{F}_j - \mathcal{F}_{j-1}}{r_j - r_{j-1}} \right), \quad (50)$$

$$\left. \frac{\partial^2 \mathcal{F}}{\partial r^2} \right|_{r_j} \approx \frac{2}{r_{j+1} - r_{j-1}} \left(\frac{\mathcal{F}_{j+1} - \mathcal{F}_j}{r_{j+1} - r_j} - \frac{\mathcal{F}_j - \mathcal{F}_{j-1}}{r_j - r_{j-1}} \right). \quad (51)$$

We can use these formulas in (25)–(28) to obtain linear systems of equations, which can be solved numerically assuming appropriate boundary conditions are known. Equations (25) and (26) for $\phi_{\ell,m}$ and $A_{\ell,m}^{\text{ind},Y}$ are coupled, so they will form one system of $2N$ linear equations. Equation (27) for $A_{\ell,m}^{\text{ind},\Phi}$ is uncoupled from the other equations and will therefore become a system of N linear equations. Finally, Eq. (28) combined

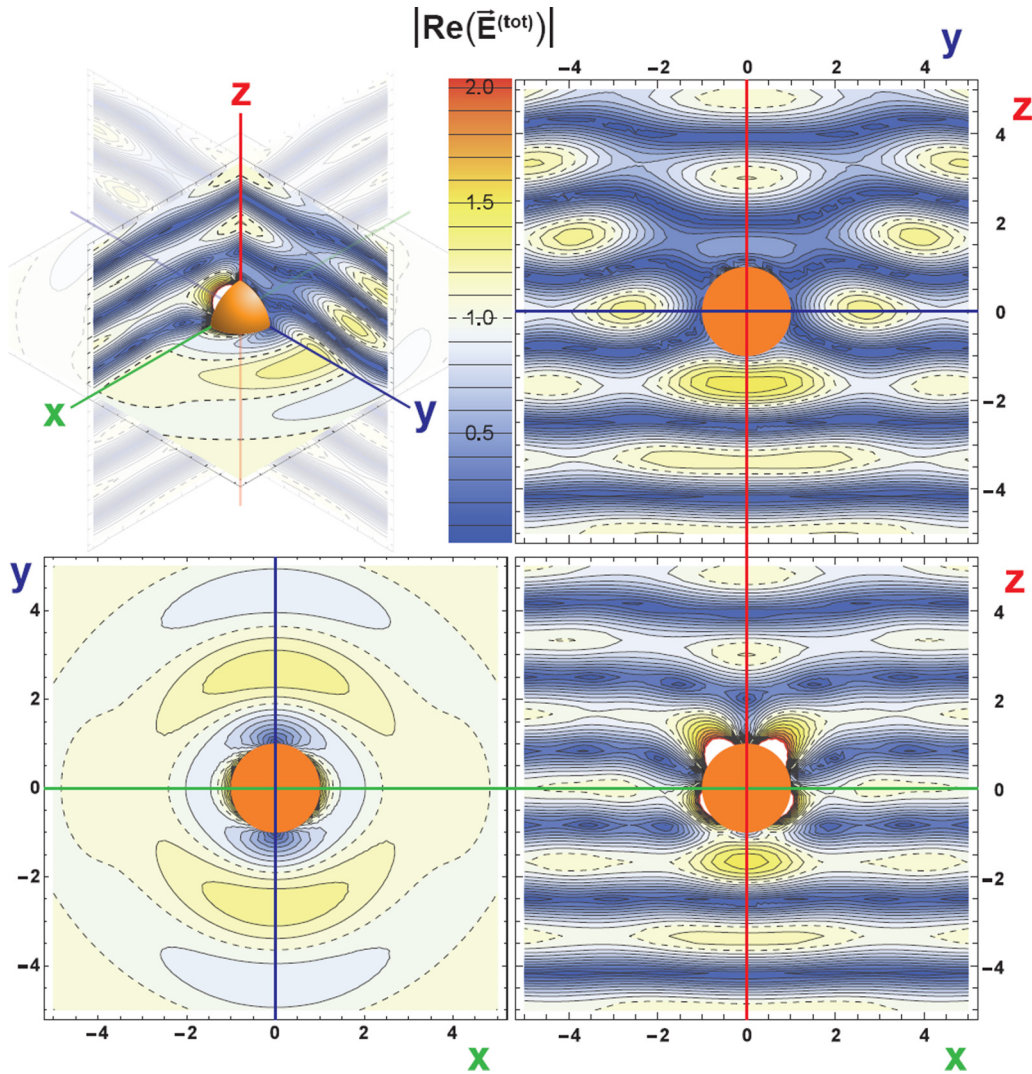


FIG. 1. The electric field nearby a gold sphere is plotted in several planes. The incoming wave arrives from the $-z$ direction and is polarized along the x direction. Units are given in $R = 150$ nm (the radius of the sphere). The calculations are performed with $\lambda = 500$ nm ($\omega = 2.48$ eV) and $\kappa = (0.662 + 4.393i) \times 10^7$ m $^{-1}$.

with (50) allows for direct calculation of $A_{\ell,m}^{\text{ind},\Psi}$, assuming the solution for $A_{\ell,m}^{\text{ind},Y}$ has already been found.

As an example, consider the following model density profile [6,10]:

$$f(r) = \frac{c_0}{\exp\left(\frac{2(r-R)}{\delta}\right) + 1}, \quad (52)$$

where the normalization constant c_0 is introduced to keep the total number of electrons fixed. It satisfies

$$c_0^{-1} = \frac{3}{R^3} \int_0^{+\infty} \frac{r^2}{\exp\left(\frac{2(r-R)}{\delta}\right) + 1} dr. \quad (53)$$

This profile represents a spherically symmetric particle with radius R , but with a smooth electron density at its interface rather than an abrupt transition. The parameter δ represents the typical length over which the electron density varies. We will refer to it as the “spill-out length.” As one might expect, the limit $\delta \rightarrow 0$ represents an abrupt interface, meaning the

results will reduce to the standard results of Mie theory. In principle, one needs $f'(0) = 0$ to have a continuous density profile in 3D: we choose $\delta \ll R$ to approximately satisfy this condition.

A problem that was encountered when solving the equations numerically is that the coupled equations for $\phi_{\ell,m}$ and $A_{\ell,m}^{\text{ind},Y}$ numerically behave badly in regions where $f'(r)$ is large in absolute value. This makes the equations hard to solve in the limit $\delta \rightarrow 0$. To solve this problem, more grid points have to be added to ensure the grid spacing is at least an order of magnitude smaller than δ , which makes the computational time much longer and the results unreliable. Fortunately, a faster and more accurate method was found.

If $f'(r) \approx 0$, Eqs. (25) and (26) decouple and analytical solutions to Eqs. (25)–(28) are known. Therefore, we do not need to discretize our equations in regions where $f'(r) \approx 0$, simplifying the problem greatly. In our case, $f'(r) \approx 0$ as $r \rightarrow 0$ or $r \rightarrow +\infty$. Therefore, our grid only needs to extend from $[r_{\min}, r_{\max}]$, where r_{\min} and r_{\max} are chosen to ensure

that outside $[r_{\min}, r_{\max}]$, $|f'(r)|$ is sufficiently small. Equations (25)–(28) are then solved similarly to the method outlined in Sec. III to obtain

$$\phi_{\ell,m}(r < r_{\min}) = c\phi_{<}(kr)^\ell, \quad (54)$$

$$A_{\ell,m}^{\text{ind},Y}(r < r_{\min}) = C_{<} \frac{j_\ell(kr)}{kr} - A_{\ell,m}^{\text{ext},Y}(r) + \frac{l}{i} \phi_{<}(kr)^{\ell-1}, \quad (55)$$

$$A_{\ell,m}^{\text{ind},\Phi}(r < r_{\min}) = B_{<} j_\ell(kr) - A_{\ell,m}^{\text{ext},\Phi}(r), \quad (56)$$

$$\phi_{\ell,m}(r > r_{\max}) = c\phi_{>}(kr)^{-(\ell+1)}, \quad (57)$$

$$A_{\ell,m}^{\text{ind},Y}(r > r_{\max}) = C_{>} \frac{h_\ell(kr)}{kr} - \frac{l+1}{i} \phi_{>}(kr)^{-(\ell+2)}, \quad (58)$$

$$A_{\ell,m}^{\text{ind},\Phi}(r > r_{\max}) = B_{>} h_\ell(kr). \quad (59)$$

In these equations, $\phi_{<}$, $C_{<}$, $B_{<}$, $\phi_{>}$, $C_{>}$, and $B_{>}$ are integration constants that all have the same units as the vector potential. In general, they are not given by formulas (43) and (44), and (48) and (49). Instead, they can be found by adding the constraints that the numerical solutions for $\phi_{\ell,m}(r)$, $A_{\ell,m}^{\text{ind},Y}(r)$, and $A_{\ell,m}^{\text{ind},\Phi}(r)$ and their derivatives are continuous at $r = r_{\min}$ and $r = r_{\max}$. Note that, in contrast to standard Mie results, $\phi'_{\ell,m}(r)$ is continuous because we use a continuous density profile function.

We combine these boundary conditions with the equations from the discretization of Eqs. (25)–(27) on a grid covering $[r_{\min}, r_{\max}]$. This gives a system of $2N + 4$ linear equations for the variables $\phi_{\ell,m,1}, \dots, \phi_{\ell,m,N}$, $A_{\ell,m,1}^{\text{ind},Y}, \dots, A_{\ell,m,N}^{\text{ind},Y}$, $\phi_{<}$, $\phi_{>}$, $C_{<}$, and $C_{>}$, and a system of $N + 2$ linear equations for the variables $A_{\ell,m,1}^{\text{ind},\Phi}, \dots, A_{\ell,m,N}^{\text{ind},\Phi}$, $B_{<}$, and $B_{>}$. It is now possible to solve these equations numerically to obtain $\phi_{\ell,m}(r)$, $A_{\ell,m}^{\text{ind},Y}(r)$, and $A_{\ell,m}^{\text{ind},\Phi}(r)$. To obtain the full solution for the vector potential, one may use Eq. (28) to find $A_{\ell,m}^{\text{ind},\Psi}(r)$ as well. In order to calculate the optical cross sections, however, one only needs to calculate $C_{>}$ and $B_{>}$ for every value for ℓ .

It is important to choose a finer grid in places where any of the potentials have high derivatives. It was found that the components of \mathbf{A} are well behaved and do not vary rapidly as a function of r . However, from Eq. (25) it can be derived that the derivatives of $\phi_{\ell m}$ become very high if $|1 + \chi f(r)|$ becomes small: this essentially corresponds to a longitudinal mode, since locally we have that $\varepsilon(r, \omega) \approx 0$. The minimum of $|1 + \chi f(r)|$ behaves almost like a singularity. We expect this to happen for metals, where χ typically has a large negative real part and a small imaginary part. Therefore, extra grid points need to be added in the regions where $|1 + \chi f(r)|$ is small.

B. Comparison to other methods

To test the validity of our numerical scheme, we compare our results to those found by Ruppin [7] using a different method based on a paper by Wyatt [6]. The results are typically represented by the optical cross sections. Ruppin uses

the following (unnormalized) density profile:

$$f(r) = \begin{cases} 1 & \text{if } r < R - \delta, \\ \frac{R-r+\delta}{2\delta} & \text{if } R - \delta < r < R + \delta, \\ 0 & \text{if } r > R + \delta. \end{cases} \quad (60)$$

We calculated the extinction cross section of a potassium nanoparticle with the above density profile; the results are shown in Fig. 2, together with the Mie results and the spectra calculated by Ruppin [7]. It is clear that the results from the beyond-Mie theories match quantitatively, confirming the validity of our method.

Figure 2(c) shows convergence of our results when calculated with a different number of grid points N . It shows that our results are well converged for $N \gtrsim 2000$. For the remainder of this article, we will therefore calculate our results using $N \sim 2500$.

Finally, we note that other methods are available to obtain the scattering coefficients $B_{>}$ and $C_{>}$ through solution of Eqs. (25)–(28). For example, it is possible to write down analytical expressions similar to (43) and (44), and (48) and (49), but depending on two unknown functions G_ℓ and W_ℓ [6]. These functions satisfy ordinary differential equations, which can be derived from Eqs. (25)–(28) and can be solved using a Runge-Kutta method. Another possible method is to approximate the electron density profile $f(r)$ by a piecewise constant function. The analytical solution in all of the regions with a constant $f(r)$ is known, as a function of six unknown integration constants: it is obtained with a method similar to that of Sec. III. By imposing the electromagnetic boundary conditions it is possible to set up a transfer matrix method for these integration constants, allowing us to calculate $B_{>}$ and $C_{>}$ in the usual way. Both of these methods need to take the ‘‘singularity’’ of the local longitudinal mode (discussed in Sec. IV A) into account. When implemented correctly, these methods may be more efficient in calculating optical cross sections. Here we chose the finite difference method to obtain the full solution for the electromagnetic potentials. In contrast, the two methods described above only focus on the asymptotic scattered field. In addition to this, we expect the finite difference method to be easier to generalize to the problem of nonlocal response [8–11].

V. BOUNDARY SOFTENING ENHANCES ABSORPTION

In the previous section a method was outlined to find the coefficients $B_{>}$ and $C_{>}$ numerically in case of a soft-interface sphere. In this section we use this method to study how the various cross sections are affected by the smoothing of the charge density at the edge of the nanosphere. These cross sections are calculated with the same formulas as those of Mie theory, since our resulting far field has the same functional form as that of a hard-walled nanosphere.

Figure 3 shows the total, scattering, and absorption cross sections of a $R = 15$ nm nanosphere for different values of the spill-out length δ . In all cases the peaks widen and undergo a redshift as δ increases. Additionally, the amplitudes of the peaks change. For the extinction and scattering cross sections, all peaks lower in amplitude until they disappear as δ increases. For the absorption, the change is more complicated: peaks associated with higher ℓ values tend to decrease in

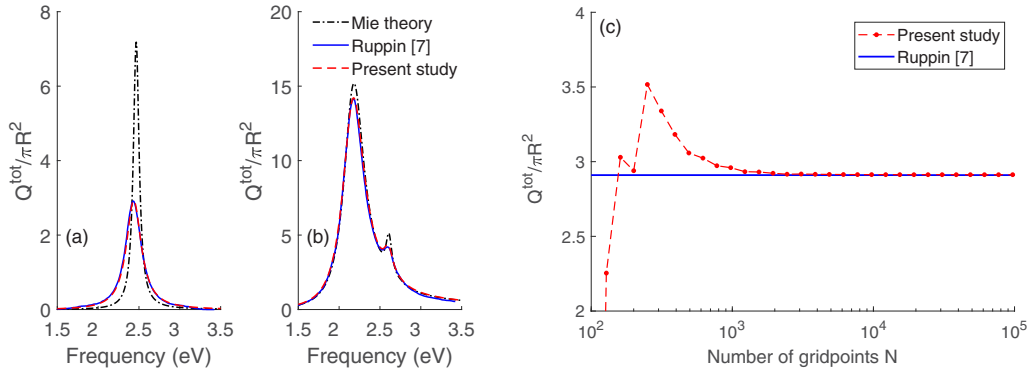


FIG. 2. Comparison of the extinction cross-section spectra from the present study and those from [7], for a potassium nanosphere with: (a) $R = 5$ nm, $\delta = 0.1$ nm; (b) $R = 50$ nm, $\delta = 0.2$ nm. Standard Drude response with $\omega_{\text{pl}} = 4.28$ eV and $1/\tau = 0.02\omega_{\text{pl}}$ was used. The results show a quantitative match and reveal the difference with the Mie result ($\delta \rightarrow 0$). (Right) (c) Convergence with respect to the amount of grid points, for the same material values as (a) and $\omega = 2.43$ eV.

amplitude and disappear, while peaks with lower ℓ values first increase in amplitude, reach a maximum, and then decrease again.

The insets show the cross sections integrated over the frequency, relative to the result from Mie theory:

$$Q_{(\text{int})}^i(\delta) := \frac{\int [Q^i(\delta, \omega) - Q_{(\text{Mie})}^i(\omega)] d\omega}{\int Q_{(\text{Mie})}^i(\omega) d\omega}. \quad (61)$$

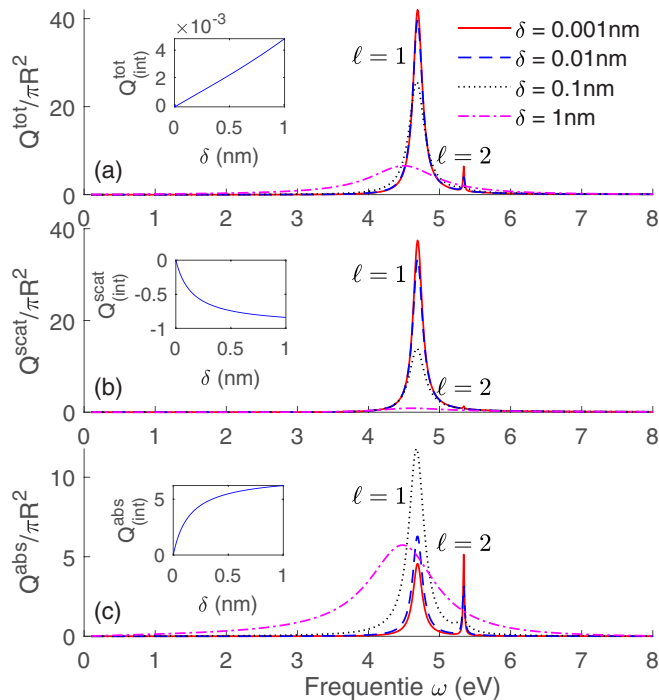


FIG. 3. (a) Total, (b) scattering, and (c) absorption cross-section spectra of a gold nanosphere with $R = 15$ nm and various spill-out lengths. Standard Drude response with $\omega_{\text{pl}} = 8.55$ eV and $1/\tau = 0.0184$ eV was used. For $\delta = 0.001$ nm the results are essentially the same as for a hard-walled sphere: several peaks associated with a value of the angular momentum ℓ . The insets show the cross sections integrated over all frequencies shown in the plot, relative to the integrated cross section from Mie theory (see text).

These integrated cross sections are dimensionless and are only a function of δ . Therefore, they are useful for the interpretation of a continuous change in the spill-out length. It is noteworthy that the integrated scattering cross section decreases quite steeply, while the integrated absorption cross section increases by about the same amount. This leads to the remarkable fact that the integrated total cross section is nearly unchanged by boundary softening.

In order to get a further understanding of what an artificially large continuous change in δ does to the absorption, a contour plot of the absorption cross section of a large nanosphere as a function of the frequency and the spill-out length was made and shown in Fig. 4. This figure clearly shows that the overall absorption increases as the boundary is smoothed, while at the same time redshifting the frequency range where absorption is strongest. This is favorable in applications where the absorption cross section needs to be maximized: once nanospheres with a chosen spill-out length can be manufactured, one can adjust this parameter to increase

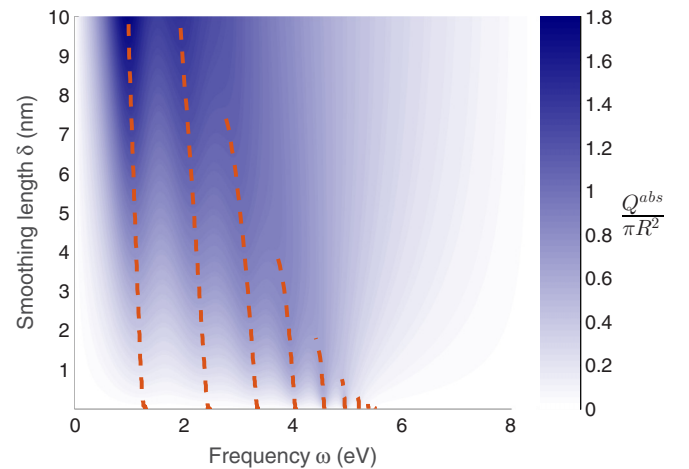


FIG. 4. Contour plot of the absorption cross section of a gold nanosphere with $R = 150$ nm. Standard Drude response with $\omega_{\text{pl}} = 8.55$ eV and $1/\tau = 0.0184$ eV was used. Every horizontal line of this plot is an absorption spectrum for a certain value of δ . The dashed lines indicate the location of the peaks of the absorption spectra.

absorption. For higher values of the spill-out length, the absorption mainly takes place for lower frequencies; this is not only due to the fact that every peak redshifts, but mostly because the low-frequency peaks increase in amplitude while the high-frequency peaks decrease in amplitude. This also implies that the absorption spectra for high values of δ are in essence different than the Mie spectra: while the absorption of a hard-walled sphere is dominated by sharp high-frequency peaks, the peaks in the absorption spectrum of a sphere with a smooth boundary are wide and occur at lower frequencies.

VI. CONCLUSIONS

Mie theory and its extensions are commonly derived using Maxwell's equations for the electric and magnetic fields. Here we provide an alternative derivation, based on the vector potential and the scalar potential. The interest in rederiving old results in a new manner lies in that this can open the way for new applications or different generalizations. The derivation considers the free electrons explicitly rather than assuming a response function, which facilitates the comparison with other nonlocal response theories. In the differential equations (25)–(28) for the scalar and vector potential, the transition between the metal and the medium is described by a density profile function $f(r)$, so that these equations do not require imposing the usual hard-wall electromagnetic boundary conditions. Thus, the equations can be applied also to soft or diffuse interfaces where the density varies radially on a scale comparable to the wavelength. The idea of using the \mathbf{Y} , $\mathbf{\Psi}$, $\mathbf{\Phi}$ vector spherical harmonics to study scattering from spheres with a smooth surface can be applied to a handful

of problems. These problems include the more complicated hydrodynamic Drude model for nanoplasmonics [8–11], scattering from nanospheres made of metamaterials [28,29], and quantum wave scattering [30–32].

When we do replace the profile function by a step function, the results from Mie theory appear. Analytic results for the hard-wall case have been found, and a numerical scheme has been proposed to solve the equations for a nanosphere with a smooth boundary. The main effect of the smoothing of the boundary is that the overall absorption cross section increases, while the resonant modes of the sphere occur at lower frequencies. For large nanospheres with large smoothing, this effect is drastically enhanced by the disappearance of the sharp, high-frequency resonant modes. Artificially increasing the absorptance of nanoparticles is important in many applications such as thermotherapy [33–35]. Our results provide a way to enhance the absorption in nanoparticles through depth-dependent doping or by using many-shell particles to create the optimal charge density profile in the particle.

ACKNOWLEDGMENTS

This research was funded by a Ph.D. grant of the Agency for Innovation by Science and Technology (IWT). N.V.d.B. acknowledges support by the Flemish Research Foundation (FWO-VI), Projects No. G.0115.12N, No. G.0119.12N, No. G.0122.12N, and No. G.0429.15N and by the Scientific Research Network of the Research Foundation-Flanders, WO.033.09N. M.H. acknowledges support from the University Research Fund (BOF) of the Antwerp University (Project ID: 38499).

-
- [1] G. Mie, Beiträge zur optik trüber medien, speziell kolloidaler metallösungen, *Ann. Phys. (Leipzig)* **330**, 377 (1908).
 - [2] J. A. Stratton, *Electromagnetic Theory* (McGraw-Hill, New York, 1941).
 - [3] M. Kerker, *The Scattering of Light and Other Electromagnetic Radiation* (Academic, New York, 1969).
 - [4] U. Kreibig and M. Vollmer, *Optical Properties of Metal Clusters* (Springer, Berlin, 1995).
 - [5] C. F. Bohren and D. R. Huffman, *Absorption and Scattering of Light by Small Particles* (Wiley, Berlin, 2004).
 - [6] P. J. Wyatt, Scattering of electromagnetic plane waves from inhomogeneous spherically symmetric objects, *Phys. Rev.* **127**, 1837 (1962); **134**, AB1 (1964).
 - [7] R. Ruppin, Optical properties of a metal sphere with a diffuse surface, *J. Opt. Soc. Am.* **66**, 449 (1976).
 - [8] G. Toscano, J. Straubel, A. Kwiatowski, C. Rockstuhl, F. Evers, H. Xu, N. A. Mortensen, and M. Wubs, Resonance shifts and spill-out effects in self-consistent hydrodynamic nanoplasmonics, *Nat. Commun.* **6**, 7132 (2015).
 - [9] N. A. Mortensen, S. Raza, M. Wubs, T. Søndergaard, and S. I. Bozhevolnyi, A generalized non-local optical response theory for plasmonic nanostructures, *Nat. Commun.* **5**, 3809 (2014).
 - [10] C. Ciraci and F. Della Sala, Quantum hydrodynamic theory for plasmonics: Impact of the electron density tail, *Phys. Rev. B* **93**, 205405 (2016).
 - [11] M. Kupresak, X. Zheng, G. A. E. Vandenbosch, and V. V. Moshchalkov, Comparison of hydrodynamic models for the electromagnetic nonlocal response of nanoparticles, *Adv. Theory Simul.* **1**, 1800076 (2018).
 - [12] R. Ruppin, Optical Properties of a Plasma Sphere, *Phys. Rev. Lett.* **31**, 1434 (1973).
 - [13] R. Ruppin, Optical properties of small metal spheres, *Phys. Rev. B* **11**, 2871 (1975).
 - [14] R. Ruppin, Plane wave interaction with a homogeneous warm plasma sphere, *Plasma Phys.* **17**, 723 (1975).
 - [15] A. R. Melnyk and M. J. Harrison, Theory of optical excitation of plasmons in metals, *Phys. Rev. B* **2**, 835 (1970).
 - [16] U. Kreibig, M. Gartz, A. Hilger, H. Hövel, M. Quinten, D. Wagner, and H. Ditlbacher, A short survey of Optical Properties of Metal Nanostructures, in *Functional Properties of Nanostructured Materials*, edited by R. Kassing, P. Petkov, W. Kulisch, and C. Popov, Nato Science Series, II. Mathematics, Physics and Chemistry, Vol. 223 (Springer, Dordrecht, The Netherlands, 2005).
 - [17] N. J. Hogan, A. S. Urban, C. Ayala-Orozco, A. Pimpinelli, P. Nordlander, and N. J. Halas, Nanoparticles heat through light localization, *Nano Lett.* **14**, 4640 (2014).
 - [18] F. Abelès, Recherches sur la propagation des ondes électromagnétiques sinusoidales dans les milieux stratifiés, *Ann. Phys. (Paris)* **12**, 706 (1950).

- [19] R. Diamant and M. Fernandez-Guasti, Light propagation in 1D inhomogeneous deterministic media: The effect of discontinuities, *J. Opt. A: Pure Appl. Opt.* **11**, 045712 (2009).
- [20] J. B. Pendry, A. J. Holden, D. J. Robbins, and W. J. Stewart, Magnetism from conductors and enhanced nonlinear phenomena, *IEEE Trans. Microw. Theory Tech.* **47**, 2075 (1999).
- [21] D. R. Smith, W. J. Padilla, D. C. Vier, S. C. Nemat-Nasser, and S. Schultz, Composite Medium with Simultaneously Negative Permeability and Permittivity, *Phys. Rev. Lett.* **84**, 4184 (2000).
- [22] D. R. Smith, J. B. Pendry, and M. C. K. Wiltshire, Metamaterials and negative refractive index, *Science* **305**, 788 (2004).
- [23] D. R. Smith, J. J. Mock, A. F. Starr, and D. Schurig, Gradient index metamaterials, *Phys. Rev. E* **71**, 036609 (2005).
- [24] J. M. Geffrin, B. García-Cámara, R. Gómez-Medina, P. Albella, L. S. Froufe-Pérez, C. Eyraud, A. Litman, R. Vaillon, F. González, M. Nieto-Vesperinas, J. J. Sáenz, and F. Moreno, Magnetic and electric coherence in forward- and back-scattered electromagnetic waves by a single dielectric subwavelength sphere, *Nat. Commun.* **3**, 1171 (2012).
- [25] S. Raza, S. I. Bozhevolnyi, M. Wubs, and N. A. Mortensen, Nonlocal optical response in metallic nanostructures, *J. Phys.: Condens. Matter* **27**, 183204 (2015).
- [26] R. G. Barrera, G. A. Estevez, and J. Giraldo, Vector spherical harmonics and their application to magnetostatics, *Eur J. Phys.* **6**, 287 (1985).
- [27] B. Carrascal, G. A. Estevez, P. Lees, and V. Lorenzo, Vector spherical harmonics and their application to classical electrodynamics, *Eur. J. Phys.* **12**, 184 (1991).
- [28] Z. Liu, Z. Lin, and S. T. Chui, Electromagnetic scattering by spherical negative-refractive-index particles: Low-frequency resonance and localization parameters, *Phys. Rev. E* **69**, 016619 (2004).
- [29] T. J. Arruda, F. A. Pinhero, and A. S. Martinez, Electromagnetic energy within coated spheres containing dispersive metamaterials, *J. Opt.* **14**, 065101 (2012).
- [30] B. Liao, M. Zebarjadi, K. Esfarjani, and G. Chen, Cloaking Core-Shell Nanoparticles from Conducting Electrons in Solids, *Phys. Rev. Lett.* **109**, 126806 (2012).
- [31] R. Fleury and A. Alù, Quantum cloaking based on scattering cancellation, *Phys. Rev. B* **87**, 045423 (2013).
- [32] C. Valagiannopoulos, Maximal quantum scattering by homogeneous spherical inclusions, *Phys. Rev. B* **100**, 035308 (2019).
- [33] L. R. Hirsch, R. J. Stafford, J. A. Bankson, S. R. Sershen, B. Rivera, R. E. Price, J. D. Hazle, N. J. Halas, and J. L. West, Nanoshell-mediated near-infrared thermal therapy of tumors under magnetic resonance guidance, *Proc. Natl. Acad. Sci.* **100**, 13549 (2003).
- [34] C. Loo, A. Lowery, N. Halas, J. West, and R. Drezek, Immunotargeted nanoshells for integrated cancer imaging and therapy, *Nano Lett.* **5**, 709 (2005).
- [35] E. Boisselier and A. Didier, Gold nanoparticles in nanomedicine: preparations, imaging, diagnostics, therapies and toxicity, *Chem. Soc. Rev.* **38**, 1759 (2009).